Determining the Velocity Fine Structure by a Laser Anemometer with Fixed Orientation

Kristensen, Leif; Kirkegaard, Peter; Mikkelsen, Torben

Publication date:
2011

Document Version
Publisher's PDF, also known as Version of record

Determining the Velocity Fine Structure by a Laser Anemometer with Fixed Orientation

Risø-R-Report

Leif Kristensen, Peter Kirkegaard,Torben Mikkelsen
Risø-R-1762(EN)
February 2011

Risø DTU
National Laboratory for Sustainable Energy

Author: Leif Kristensen, Peter Kirkegaard, Torben Mikkelsen
Title: Determining the Velocity Fine Structure by a Laser Anemometer with Fixed Orientation
Division: Wind Energy Division

Risø-R-1762(EN)
February 2011

Abstract (max. 2000 char.):

We have studied the velocity structure functions and spectra which can be determined by a CW-laser anemometer and a (pulsed) lidar anemometer. We have found useful theoretical expressions for both types of anemometers and compared their filtering of the along-beam turbulent velocity. The purpose has been to establish a basis for remote determining of turbulence fine-structure in terms of the rate of dissipation of specific kinetic energy in the atmospheric boundary layer.

ISSN 0106-2840
ISBN 978–87–550–3840-0

Contract no.:

Group's own reg. no.:
1130408-01

Sponsorship:
Danish Strategic Research Council, grant no. 2104-05-0076

Cover :

Pages: 32
Tables: 2
References: 8

Information Service Department
Risø National Laboratory for Sustainable Energy
Technical University of Denmark
P.O.Box 49
DK-4000 Roskilde
Denmark
Telephone +45 46774005
bibl@risoe.dtu.dk
Fax +45 46774013
www.risoe.dtu.dk

Contents

1 Introduction

The technical developments over the last decade has made it possible to construct robust, affordable and reliable Doppler laser anemometers. When pointing the laser into the air the light is scattered in all directions by aerosols and that part of the light, which is reflected into the laser receiver, can be analyzed to determine its power spectrum, the Doppler spectrum. Since the aerosols are in motion the light will change frequency corresponding to the average velocity in a volume, which for most practical applications can be considered a finite line segment aligned the beam direction. The shift in mean frequency, determined by the outgoing and the incoming Doppler spectra, is proportional to the velocity component along the beam direction. Smalikho (1995) discussed this phenomenon in details. There are two modes of laser operation, continuous or pulsed. In the first case the laser is operating continuously and focused at a particular distance. This type of instrument, the CW-laser anemometer, is one subject of the following. We rely heavily on the pioneering work by Smalikho (1995) and Banakh & Smalikho (1997). In the second case being discussed each pulse is analyzed and the distance to the measuring volume is determined by means of pulse time-of-flight. This technique is termed range gating and has the advantage that the velocity can be measured simultaneously at several distances. In both cases the velocity is averaged over a line segment along the laser beam. Here we shall call the first type of instrument a CW-laser anemometer (Continous-Wave laser anemometer) and the second a LIDAR anemometer (LIght Detection And Ranging anemometer). The general purpose of this investigation is to obtain expressions for the structure function with small displacements and velocity spectra at corresponding large wave number. First, however, we shall take a closer look at the inherently embedded low-pass filters for the two types of laser anemometers.

2 Line Averaging

The line averaging is characterized by a distance R from the lidar and a characteristic length, ℓ of the averaging function $h(R, \ell, x)$. If we call the unfiltered velocity component along the beam $u_\circ(x)$ then the filtered velocity can be written

$$u(x) = \int_{-\infty}^{\infty} h(R, \ell, x')\, u_\circ(x - x')\, \mathrm{d}x', \tag{1}$$

where

$$\int_{-\infty}^{\infty} h(R, \ell, x')\, \mathrm{d}x' = 1. \tag{2}$$

The Fourier transform of $u_\circ(x)$ and $u(x)$ are defined as

$$\widehat{u}_\circ(k) = \frac{1}{2\pi} \int_{-\infty}^{\infty} u_\circ(x)\, \mathrm{e}^{\mathrm{i}kx}\, \mathrm{d}x \tag{3}$$

and

$$\widehat{u}(k) = \frac{1}{2\pi} \int_{-\infty}^{\infty} u(x)\, \mathrm{e}^{\mathrm{i}kx}\, \mathrm{d}x, \tag{4}$$

respectively.

We obtain a relation between $\widehat{u}(k)$ and $\widehat{u}_\circ(k)$ by substituting (1) in (4), changing the orders of integration, and applying the inverse Fourier transformation

$$u_\circ(x) = \int_{-\infty}^{\infty} \widehat{u}_\circ(k)\, \mathrm{e}^{-\mathrm{i}kx}\, \mathrm{d}k. \tag{5}$$

This process runs as follows:

$$\begin{aligned}
\widehat{u}(k) &= \frac{1}{2\pi} \int_{-\infty}^{\infty} \mathrm{e}^{ikx}\, \mathrm{d}x \int_{-\infty}^{\infty} h(R, \ell, x')\, u_\circ(x - x')\, \mathrm{d}x' \\
&= \int_{-\infty}^{\infty} h(R, \ell, x')\, \mathrm{d}x' \frac{1}{2\pi} \int_{-\infty}^{\infty} u_\circ(x - x')\, \mathrm{e}^{ikx}\, \mathrm{d}x\, \mathrm{e}^{-\mathrm{i}k'(x-x')}\, \mathrm{d}k' \\
&= \int_{-\infty}^{\infty} h(R, \ell, x')\, \mathrm{d}x' \int_{-\infty}^{\infty} \widehat{u}_\circ(k')\, \mathrm{e}^{\mathrm{i}k'x'}\, \mathrm{d}k' \underbrace{\frac{1}{2\pi} \int_{-\infty}^{\infty} \mathrm{e}^{i(k-k')x}\, \mathrm{d}x}_{\delta(k-k')} \\
&= \widehat{h}(R, \ell, k)\, \widehat{u}_\circ(k),
\end{aligned} \tag{6}$$

where

$$\widehat{h}(R, \ell, k) = \int_{-\infty}^{\infty} h(R, \ell, x)\, \mathrm{e}^{ikx}\, \mathrm{d}x \tag{7}$$

is the amplitude transfer function. A spectrum is proportional to the absolute square of the Fourier amplitudes so the spectral transfer function is in general

$$H(\ell, R, \ell, k) = |\widehat{h}(R, \ell, k)|^2 = \left| \int_{-\infty}^{\infty} h(R, \ell, x)\, \mathrm{e}^{ikx}\, \mathrm{d}x \right|^2. \tag{8}$$

2.1 The CW-Laser Anemometer

The laser light is focused at a particular distance R. In this case the two length scales R and ℓ are interrelated. Following Smalikho (1995) we have, in our notation, the line averaging function

$$h(R, x) = \frac{1}{\pi R} \frac{\mu}{\mu^2 (1 - x/R)^2 + (x/R)^2}, \tag{9}$$

where the dimensionless parameter

$$\mu = k_\circ a_\circ^2 / R \tag{10}$$

is defined in terms of the wave number $k_\circ$ of the laser radiation and the exit radius of the laser aperture $a_\circ$.

We may recast (9) in the simple Cauchy bell shape:

$$h(R,x) = \frac{1}{\pi R} \frac{\mu}{(1+\mu^2)\left(\dfrac{\mu^2}{1+\mu^2} - \dfrac{x}{R}\right)^2 + \dfrac{\mu^2}{1+\mu^2}}. \tag{11}$$

The integral of this weighting function is not, as expected, equal to one, since

$$J = \int_0^\infty h(R,x)\,\mathrm{d}x = \frac{1}{2} + \frac{\arctan(\mu)}{\pi}. \tag{12}$$

However, in the limit $\mu \to \infty$ we get

$$J \simeq 1 - \frac{1}{\pi\mu}. \tag{13}$$

According to Smalikho (1995) μ is indeed very large so the normalization is, from practical point of view, equal to 1. We may in this limit simplify (9) to

$$h(R,x) = \frac{1}{\pi R} \frac{\mu}{\mu^2\left(1 - \dfrac{x}{R}\right)^2 + 1}. \tag{14}$$

This equation shows that the weighting function has its maximum at $x = R$. The full width half maximum (FWHM) is attained at the distances $x = R \pm R/\mu$, which defines the characteristic length scale

$$\ell = 2\,\frac{R}{\mu} = 2\,\frac{R^2}{k_\circ a_\circ^2}. \tag{15}$$

In this case the spectral transfer function becomes

$$H(\ell,k) = \exp(-\ell|k|). \tag{16}$$

2.2 The LIDAR Anemometer

Here the range gating is carried out by averaging the return signal from the pulse *, assumed Gaussian, over the time from $T - \Delta t/2$ to $T + \Delta t/2$. For an unweighted gate we get in this time interval the contribution from the distance $x = ct/2$

$$h(T,\Delta t,\sigma,x) = \frac{1}{\Delta t} \int_{T-\Delta t/2}^{T+\Delta t/2} \exp\left(-\frac{(x - ct'/2)^2}{2\sigma^2}\right) \frac{\mathrm{d}t'}{\sqrt{2\pi}\sigma}, \tag{17}$$

*Since the pulse must travel out and back, the detected signal has effectively traveled with half the speed of light $c/2$.

where σ characterizes the spatial width (Gaussian standard deviation) of the pulse.

Since it is more convenient to work in spatial rather than temporal coordinates, we introduce the notation

$$\left\{ \begin{array}{c} x' \\ R \\ L \end{array} \right\} = \left\{ \begin{array}{c} ct'/2 \\ cT/2 \\ c\Delta t/2 \end{array} \right\}, \tag{18}$$

where R, as in the case of the CW-laser anemometer, is the distance to the middle of the pulse, and we get for the laser anemometers sampling function along the line of sight

$$\begin{aligned} h(R,L,\sigma,x) &= \frac{1}{L}\int_{R-L/2}^{R+L/2} \exp\left(-\frac{(x-x')^2}{2\sigma^2}\right)\frac{\mathrm{d}x'}{\sqrt{2\pi}\sigma} \\ &= \frac{1}{2L}\left\{\mathrm{erf}\left(\frac{R-x+L/2)}{\sqrt{2}\sigma}\right) - \mathrm{erf}\left(\frac{R-x-L/2}{\sqrt{2}\sigma}\right)\right\}. \end{aligned} \tag{19}$$

To obtain the amplitude spectral transfer function it is most convenient to insert the first part (9), the integral, in (7). By interchanging the order of integration we get

$$\begin{aligned} \widehat{h}(R,L,\sigma,k) &= \int_{-\infty}^{\infty} h(R,L,\sigma,x)\,\mathrm{e}^{\,\mathrm{i}kx}\mathrm{d}x \\ &= \mathrm{e}^{\,\mathrm{i}kR}\ \mathrm{sinc}\left(\frac{kL}{2}\right)\exp\left(-\frac{\sigma^2k^2}{2}\right), \end{aligned} \tag{20}$$

where, by definition,

$$\mathrm{sinc}(s) = \frac{\sin s}{s}. \tag{21}$$

The spectral transfer function then becomes

$$H(L,\sigma,k) = \left|\widehat{h}(R,L,\sigma,k\right|^2 = \mathrm{sinc}^2\left(\frac{kL}{2}\right)\exp\left(-\sigma^2k^2\right). \tag{22}$$

For our purpose it is sufficiently accurate to expand the first factor and reformulate it according to the scheme

$$\mathrm{sinc}^2\left(\frac{x}{2}\right) \approx \left(1-\frac{(x/2)^2}{6}\right)^2 \approx 1-\frac{x^2}{12} \approx \exp\left(-\frac{x^2}{12}\right). \tag{23}$$

We introduce a combined length scale

$$\ell = \sqrt{\frac{L^2}{12}+\sigma^2} \tag{24}$$

and write (22) as

$$H(\ell,k) = \exp\left(-\ell^2k^2\right). \tag{25}$$

3 Fixed-Beam Configuration

The configuration is described in Fig. 1. Here $\boldsymbol{t}$ is the beam direction and $\boldsymbol{U}$ the mean wind speed. Applying Taylor's frozen-turbulence hypothesis, we see that the laser is probing the instantaneous velocity field along lines which are displaced $\boldsymbol{U}(t_2 - t_1)$ from the time t_1 to the time t_2. We define the beam direction $\boldsymbol{t}$ as the $\boldsymbol{i}_1$ axis in the Cartesian coordinate system. The two other unit axes defining the coordinate system are

$$\boldsymbol{i}_3 = \frac{\boldsymbol{t} \times \boldsymbol{U}}{|\boldsymbol{t} \times \boldsymbol{U}|} = \frac{\boldsymbol{t} \times \boldsymbol{r}}{|\boldsymbol{t} \times \boldsymbol{r}|} \tag{26}$$

and

$$\boldsymbol{i}_2 = \boldsymbol{i}_3 \times \boldsymbol{i}_1. \tag{27}$$

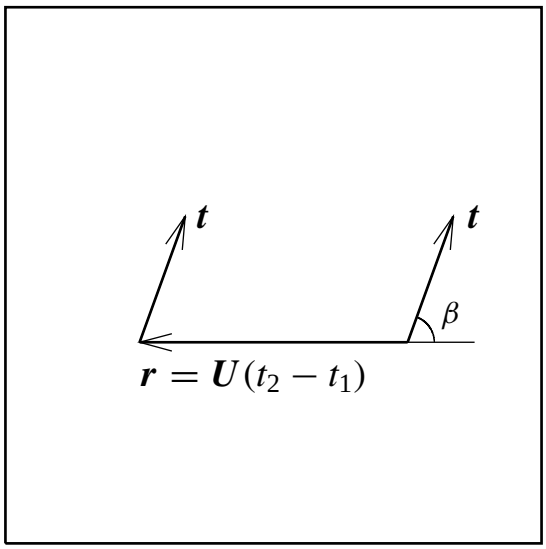

Figure 1. Parallel beam situation. The displacement $\boldsymbol{r}$ between measurements is entirely due to eddy transport by the mean wind velocity $\boldsymbol{U}$.

We want to determine the structure function between the velocity components along $\boldsymbol{t} = \boldsymbol{i}_1$ and follow the approach by Smalikho (1995) who makes his derivation via the spectral formulation. The spectral tensor for isotropic turbulence is

$$\Phi_{ij}(\boldsymbol{k}) = \frac{E(k)}{4\pi k^2}\left\{\delta_{ij} - \frac{k_i k_j}{k^2}\right\}, \qquad \left.\begin{matrix} i \\ j \end{matrix}\right\} = 1, 2, 3, \tag{28}$$

where

$$\boldsymbol{k} = k_1\boldsymbol{i}_1 + k_2\boldsymbol{i}_2 + k_3\boldsymbol{i}_3, \tag{29}$$

and

$$k = |\boldsymbol{k}| = \sqrt{k_1^2 + k_2^2 + k_3^2}. \tag{30}$$

The filtered spectral tensor is

$$\overline{\Phi}_{ij}(\boldsymbol{k}) = \Phi_{ij}(\boldsymbol{k})\, H(\ell, k_1), \tag{31}$$

where $H(\ell, k_1)$ can be either of the spectral transfer functions (16) and (25). The filtered covariance of the velocity components along $\boldsymbol{t}$ and the displacement

$$\boldsymbol{r} = r\{-\cos\beta\, \boldsymbol{i}_1 + \sin\beta\, \boldsymbol{i}_2\}, \tag{32}$$

where $\pi - \beta$ is the angle from $\boldsymbol{t}$ to $\boldsymbol{r}$ (see Fig. 1), is

$$\begin{aligned}\overline{\mathcal{R}}(\ell, r, \beta) = \overline{R}_{11}(\boldsymbol{r}) &= \int \mathrm{d}^3k\, \overline{\Phi}_{11}(\boldsymbol{k}) \exp(\mathrm{i}\,\boldsymbol{k}\cdot\boldsymbol{r}) \\ &= \int \mathrm{d}^3k\, \frac{E(k)}{4\pi k^2} \left\{1 - \frac{k_1^2}{k^2}\right\} H(\ell, k_1) \exp(-\mathrm{i}\, r\{k_1\cos\beta - k_2\sin\beta\})\,. \end{aligned} \tag{33}$$

Since there are only two variables, r and β, it is convenient, in view of the definition (32), to use them instead of the vector argument.

Changing the integration variables by

$$\left\{ \begin{array}{c} k_1 \\ k_2 \end{array} \right\} = K \left\{ \begin{array}{c} \cos\Theta \\ \sin\Theta \end{array} \right\} \tag{34}$$

we get

$$\begin{aligned}\overline{\mathcal{R}}(\ell, r, \beta) = &\int_0^\infty K\,\mathrm{d}K \int_0^{2\pi} \mathrm{d}\Theta \int_{-\infty}^{\infty} \mathrm{d}k_3\, \frac{E\left(\sqrt{k_3^2 + K^2}\right)}{4\pi(k_3^2 + K^2)} \\ &\left\{1 - \frac{K^2\cos^2\Theta}{k_3^2 + K^2}\right\} H(\ell, K\cos\Theta) \exp(-\mathrm{i}\, r K \cos(\Theta + \beta))\,. \end{aligned} \tag{35}$$

We consider only displacements r, which are small to the integral scale and assume local isotropy. In this case the energy spectrum has the form

$$E(k) = \alpha\varepsilon^{2/3}k^{-5/3}, \tag{36}$$

where α is the Kolmogorov constant and ε the dissipation of specific kinetic energy[†]. This means that

[†]In the atmospheric boundary layer ε will in general not be constant, but rather a function of the height z. In the neutral surface layer ε is inversely proportional to z.

$$\overline{\mathcal{R}}(\ell, r, \beta) = \frac{\alpha\varepsilon^{2/3}}{4\pi} \int_0^{2\pi} \mathrm{d}\Theta \int_0^{\infty} K\,\mathrm{d}K\, H(\ell, K\cos\Theta) \exp(-\mathrm{i}\, r K \cos(\Theta + \beta))$$

$$\times \int_{-\infty}^{\infty} \left\{ 1 - \frac{K^2 \cos^2\Theta}{k_3^2 + K^2} \right\} \frac{\mathrm{d}k_3}{(k_3^2 + K^2)^{11/6}}. \quad (37)$$

The integration with respect to k_3 can easily be carried out. The result is

$$\overline{\mathcal{R}}(\ell, r, \beta) = \alpha\varepsilon^{2/3} \frac{\Gamma(1/3)}{10\sqrt{\pi}\,\Gamma(5/6)} \int_0^{2\pi} \left\{ 1 - \frac{8}{11}\cos^2\Theta \right\} \mathrm{d}\Theta$$

$$\times \int_0^{\infty} \frac{\mathrm{d}K}{K^{5/3}} H(\ell, K\cos\Theta) \cos(r K \cos(\Theta + \beta))\,. \quad (38)$$

The exponential with the imaginary argument has been replaced by the corresponding cosine function since the covariance is real. The integral over K is divergent for any value of r, but when we, following the Russian School of meteorology (Kolmogorov 1941), introduce the structure function

$$\overline{\mathcal{D}}(\ell, r, \beta) = 2\left\{ \overline{\mathcal{R}}(\ell, 0, \beta) - \overline{\mathcal{R}}(\ell, r, \beta) \right\}, \quad (39)$$

we obtain a finite result for this quantity:

$$\overline{\mathcal{D}}(\ell, r, \beta) = \alpha\varepsilon^{2/3} \frac{\Gamma(1/3)}{5\sqrt{\pi}\,\Gamma(5/6)} \int_0^{2\pi} \left\{ 1 - \frac{8}{11}\cos^2\Theta \right\} \mathrm{d}\Theta$$

$$\times \int_0^{\infty} \frac{\mathrm{d}K}{K^{5/3}} H(\ell, K\cos\Theta) \left\{ 1 - \cos(r K \cos(\Theta + \beta)) \right\}. \quad (40)$$

Using the structure function rather than the covariance function we have the advantage that the turbulence integral scale, or the outer scale of the turbulence, is not entering the analysis because definition of the structure function implies that the contribution from large eddies are filtered out.

We now evaluate (40) for the two types of anemometers, the CW-laser anemometer and the lidar anemometer.

3.1 The CW-Laser Anemometer

It is convenient here to scale distances with the parameter ℓ, i.e. twice the Rayleigh length, and define

$$\rho = \frac{r}{\ell}. \quad (41)$$

The filtered structure function (39) can then be written

$$\overline{\mathcal{D}}(\ell, r, \beta) = \alpha(\varepsilon\ell)^{2/3} \frac{\Gamma(1/3)}{5\sqrt{\pi}\,\Gamma(5/6)} \int_0^{2\pi} \left\{1 - \frac{8}{11}\cos^2\Theta\right\} \Psi(\beta, \rho, \Theta)\,\mathrm{d}\Theta, \tag{42}$$

where

$$\Psi(\beta, \rho, \Theta) = \int_0^{\infty} \exp(-\kappa|\cos\Theta|)\,\{1 - \cos(\rho\kappa\cos(\Theta + \beta))\}\,\frac{\mathrm{d}\kappa}{\kappa^{5/3}}. \tag{43}$$

This integral can be expressed in terms of analytical functions by

$$\Psi(\beta, \rho, \Theta) = \frac{3}{2}\,\Gamma\left(\frac{1}{3}\right) \times$$

$$\left\{\left[\cos^2\Theta + \rho^2\cos^2(\Theta + \beta)\right]^{1/3} \cos\left(\frac{2}{3}\arctan\left(\rho\left|\frac{\cos(\Theta + \beta)}{\cos\Theta}\right|\right)\right) - |\cos\Theta|^{2/3}\right\}. \tag{44}$$

The equation for $\overline{\mathcal{D}}(\ell, r, \beta)$ is thus reduced to a single integral over Θ. This is evaluated numerically for a selection of the angle β and the result is shown in Fig. 2.

When $\rho \gg 1$ (44) degenerates to

$$\Psi(\beta, \rho, \Theta) \simeq \Psi(\beta, \rho \to \infty, \Theta) = \frac{3}{4}\Gamma\left(\frac{1}{3}\right)\,\rho^{2/3}\,|\cos(\Theta + \beta)|^{2/3}. \tag{45}$$

Inserting this result into (42) we get

$$\overline{\mathcal{D}}(\ell, r \to \infty, \beta) = \frac{27}{55}\,\Gamma\left(\frac{1}{3}\right)\,\alpha\,(\varepsilon\,r)^{2/3}\left(1 + \frac{1}{3}\sin^2\beta\right), \tag{46}$$

In this, somewhat unrealistic limit, where $r/\ell \gg 1$, the averaging volume can be considered of zero extension and we get, as expected, the classical result (46). It can be obtained directly from the structure function tensor for locally isotropic turbulence given by

$$D_{ij}(\boldsymbol{r}) = \{D_L(r) - D_T(r)\}\,\frac{r_i r_j}{r^2} + D_T(r)\,\delta_{ij}, \tag{47}$$

where the displacement vector $\boldsymbol{r}$ is given by (32) and where

$$D_L(r) = \frac{27}{55}\,\Gamma\left(\frac{1}{3}\right)\,\alpha\,(\varepsilon\,r)^{2/3} \tag{48}$$

and

$$D_T(r) = \frac{36}{55}\,\Gamma\left(\frac{1}{3}\right)\,\alpha\,(\varepsilon\,r)^{2/3}, \tag{49}$$

Next we consider the case $\rho \ll 1$. It can be shown (see Appendix A) that

$$\overline{\mathcal{D}}(\ell, r, \beta) \quad = \quad \alpha\,(\varepsilon\ell)^{2/3}\left\{\frac{9}{25}\sqrt{\frac{3}{\pi}}\frac{\Gamma^2(1/3)}{\Gamma(5/6)}\,(\rho\sin\beta)^{5/3}\right.$$

$$\left.+\frac{3}{55}\,\Gamma\left(\frac{1}{3}\right)\,(7\cos 2\beta - 5)\,\rho^2\right\} + \mathcal{O}\left(\rho^{11/3}\right). \tag{50}$$

In the case $\beta = 0$, i.e. when the beam is in the direction of the mean wind, (50) yields

$$\overline{\mathcal{D}}(\ell, r, 0) = \alpha(\varepsilon\ell)^{2/3}\frac{6}{55}\,\Gamma\left(\frac{1}{3}\right)\,\rho^2 + \mathcal{O}\left(\rho^{11/3}\right). \tag{51}$$

When the beam is perpendicular to the mean wind, i.e. $\beta = \pi/2$, we obtain

$$\overline{\mathcal{D}}(\ell, r, \pi/2) = \alpha(\varepsilon\ell)^{2/3}\frac{9}{25}\sqrt{\frac{3}{\pi}}\,\frac{\Gamma^2(1/3)}{\Gamma(5/6)}\,\rho^{5/3} + \mathcal{O}\left(\rho^2\right). \tag{52}$$

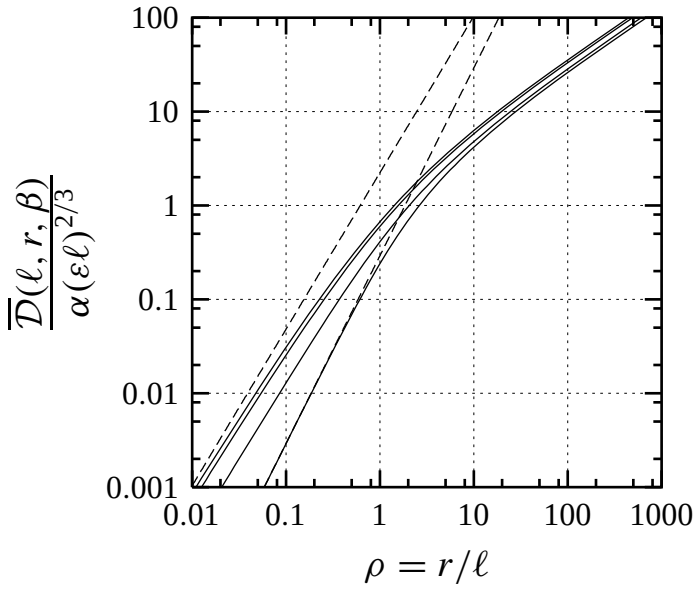

Figure 2. The normalized structure function for a CW-laser anemometer as a function of the normalized displacement. The dashed lines show the explicit formulas (51) and (52), while the numerical integration results for $\beta = 0°, 30°, 60°,$ and $90°$ are displayed with solid lines. The structure functions increase with β. Note that the numerical integration shows the limiting result (46).

Leaving out the residual terms, we may reformulate (50) in terms of a one-dimensional spectrum, $\overline{\mathcal{F}}(k, \beta)$, with the wave number in the direction of the displace vector $\boldsymbol{r}$. In general we have

$$\overline{\mathcal{D}}(\ell, r, \beta) = 4\int_0^\infty \overline{\mathcal{F}}(\ell, k, \beta)\{1 - \cos(kr)\}\mathrm{d}k. \tag{53}$$

The integral is convergent if $\overline{\mathcal{F}}(\ell, k, \beta)$ is a power law with a power in the open interval from -3 to -1. The equation shows that if $\overline{\mathcal{D}}(\ell, r, \beta)$ is proportional to $r^{\,p}$ then $\overline{\mathcal{F}}(\ell, k, \beta)$

is proportional to $k^{-(1+p)}$. The spectrum corresponding to the first term of (50) becomes

$$\overline{\mathcal{F}}_1(\ell, k, \beta) = \alpha(\varepsilon\ell)^{2/3}\frac{1}{5\sqrt{\pi}}\,\frac{\Gamma(1/3)}{\Gamma(5/6)}\,\sin^{5/3}\beta\,(k\ell)^{-8/3}\,\ell. \tag{54}$$

We see that the second term of (50) has $p = 2$. This means that the spectrum corresponding to the this term would be $-(1 + p) = -3$. The integral (53) is then divergent. The spectrum $\overline{\mathcal{F}}_2(\ell, k, \beta)$ can consequently not be a power law. However, in this case the second term is proportional to the structure function with $\beta = 0$, i.e. with the mean-wind direction along the beam. Considering only positive wave numbers, this means that the spectrum, apart from a numerical factor, has the form

$$\overline{\mathcal{F}}_2(\ell, k_1, \beta) \propto \exp(-k_1\ell)\;k_1^{-5/3}, \tag{55}$$

obtained by integrating $\overline{\Phi}_{11}(\boldsymbol{k})$ in (31) over k_2 and k_3. Combining (55) with (53) and the second term of (50), we get

$$\overline{\mathcal{F}}_2(\ell, k, \beta) = \alpha\,(\varepsilon\ell)^{2/3}\,\frac{9}{55}\,\frac{7\cos(2\beta) - 5}{2}\exp(-k\ell)\,(k\ell)^{-5/3}\ell. \tag{56}$$

The residual term $\mathcal{O}\big((r/\ell)^{11/3}\big)$ in (50) has no easily obtainable counterpart in the spectral domain in the limit $r/\ell \ll 1$. However, we assume that this part is limited by the finite scale of the turbulence and that the spectrum corresponding to (50) can be approximated by

$$\overline{\mathcal{F}}(\ell, k, \beta) = \overline{\mathcal{F}}_1(\ell, k, \beta) + \overline{\mathcal{F}}_2(\ell, k, \beta). \tag{57}$$

The first term of (57) was also found by Banakh & Smalikho (1997) and used in Banakh et al. (1999).

The spectrum is so ”steep“ that, in order to obtain a spectrum from measured time series, it will be necessary to apply tapering to exclude spectral overestimation. Kristensen et al. (1992) showed how the so-called Hanning window may remedy this.

3.2 The LIDAR Anemometer

The situation is similar to that of the continuous-wave laser anemometer and the filtered structure function has the same form as (42), i.e.

$$\overline{D}(\ell, r, \beta) = \alpha(\varepsilon\ell)^{2/3}\frac{\Gamma(1/3)}{5\sqrt{\pi}\Gamma(5/6)}\int_0^{2\pi}\left\{1 - \frac{8}{11}\cos^2\Theta\right\}\Psi(\beta, \rho, \Theta)\,\mathrm{d}\Theta, \tag{58}$$

but with

$$\Psi(\beta, \rho, \Theta) = \int_0^{\infty}\exp\Big(-\kappa^2\cos^2\Theta\Big)\,\{1 - \cos(\rho\kappa\cos(\Theta + \beta))\}\,\frac{\mathrm{d}\kappa}{\kappa^{5/3}}. \tag{59}$$

We obtain

$$\Psi(\beta, \rho, \Theta) = \frac{3}{2}\Gamma\left(\frac{2}{3}\right)|\cos\Theta|^{2/3}\left\{{}_1F_1\left(-\frac{1}{3}; \frac{1}{2}; -\frac{\rho^2}{4}\,\frac{\cos^2(\Theta + \beta)}{\cos^2\Theta}\right) - 1\right\}, \tag{60}$$

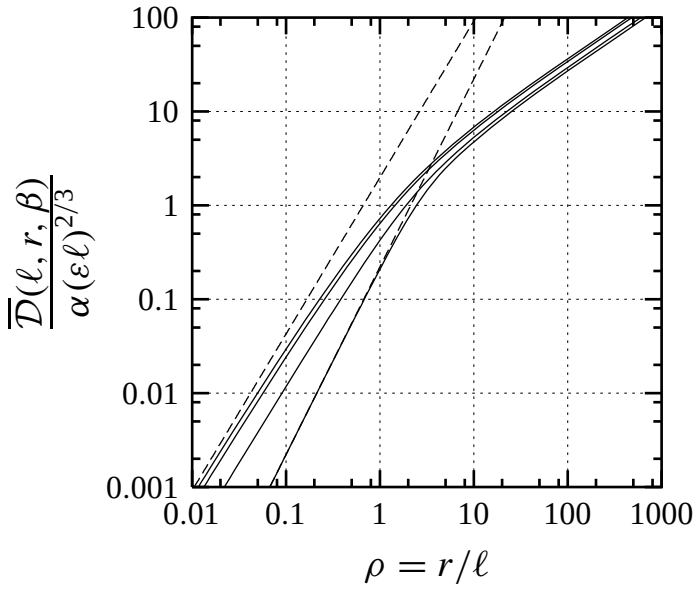

Figure 3. The normalized structure function for a LIDAR anemometer as a function of the normalized displacement. The dashed lines show the explicit formula (63) for $\beta = 0°$ and $\beta = 90°$, while the numerical integration results for $\beta = 0°, 30°, 60°,$ and $90°$ are displayed with solid lines. The structure functions increase with β. Note that the numerical integration shows the limiting result (62).

where ${}_1F_1(a, b, x)$ is the Kummer confluent hypergeometric function. Figure 3 shows the structure function for a selection of angles β.

In the limit $\rho \to \infty$ we have

$$\Psi(\beta, \rho, \Theta) \approx \frac{3}{4}\,\Gamma\left(\frac{1}{3}\right)\rho^{2/3}\,|\cos(\Theta + \beta)|^{2/3} \tag{61}$$

and, inserting in (58), we obtain again the classical result

$$\overline{\mathcal{D}}(\ell, r \to \infty, \beta) = \frac{27}{55}\,\Gamma\left(\frac{1}{3}\right)\,\alpha\,(\varepsilon\, r)^{2/3}\left(1 + \frac{1}{3}\sin^2\beta\right). \tag{62}$$

The integral (58) can be evaluated numerically.

We are particularly interested in the limit $\rho \to 0$. Appendix B is devoted to the derivation of the expression

$$\begin{aligned}\overline{\mathcal{D}}(\ell, r, \beta) \quad &\approx \quad \alpha\,(\varepsilon\ell)^{2/3}\left\{\frac{3\sqrt{3}}{25}\frac{\Gamma(1/6)\pi}{\Gamma^2(2/3)}\,(\rho\sin\beta)^{5/3}\right.\\ &\left.+\frac{9\Gamma(2/3)}{110}\,(7\cos(2\beta) - 5)\,\rho^2\right\}.\end{aligned} \tag{63}$$

As in the case of the CW laser anemometer there are two types of spectra corresponding to the two limiting terms in the structure function (63). For the $\rho^{\,5/3}$ term and the ρ^2 term they are, respectively:

$$\overline{\mathcal{F}}_1(\ell, k, \beta) = \alpha\,(\varepsilon\ell)^{2/3}\frac{\sqrt{3}}{30}\,\frac{\Gamma(1/6)}{\Gamma(2/3)}\,\sin^{5/3}\beta\,(k\ell)^{-8/3}\ell \tag{64}$$

and

$$\overline{\mathcal{F}}_2(\ell, k, \beta) = \frac{9}{110}\,\alpha\,(\varepsilon\ell)^{2/3}(7\cos(2\beta) - 5)\exp(-\ell^2k^2)(k\ell)^{-5/3}\ell. \tag{65}$$

Again, the spectrum is

$$\overline{\mathcal{F}}(\ell, k, \beta) = \overline{\mathcal{F}}_1(\ell, k, \beta) + \overline{\mathcal{F}}_2(\ell, k, \beta). \tag{66}$$

4 Validation of CW and LIDAR Anemometer Models

We can easily make a comparison between the spectra obtained by a CW-laser and a lidar for small displacements and large wave numbers, since we have explicit analytic expressions.

For the CW laser the dimensionless structure function and the spectrum are in the inertial subrange

$$\Delta(\beta, r/\ell) = \frac{\overline{\mathcal{D}}(l, r, \beta)}{\alpha(\varepsilon\ell)^{2/3}} =$$

$$\frac{9}{25}\sqrt{\frac{3}{\pi}}\frac{\Gamma^2(1/3)}{\Gamma(5/6)}\,\sin^{5/3}\beta\,(r/\ell)^{5/3} + \frac{3}{55}\Gamma\left(\frac{1}{3}\right)(7\cos(2\beta) - 5)(r/\ell)^2 \tag{67}$$

and

$$f(\beta, k\ell) = \frac{k\overline{\mathcal{F}}(\ell, k\beta)}{\alpha(\varepsilon\ell)^{2/3}} =$$

$$\frac{1}{5\sqrt{\pi}}\frac{\Gamma(1/3)}{\Gamma(5/6)}\,\sin^{5/3}\beta\,(k\ell)^{-5/3} + \frac{9}{110}(7\cos(2\beta) - 5)\exp(-k\ell)(k\ell)^{-2/3}. \tag{68}$$

For the lidar anemometer we define

$$\ell = \sqrt{\sigma^2 + \frac{L^2}{q^2}}, \tag{69}$$

where q is a dimensionless constant, which is $12^{1/2}$ for a unweighted gate of duration Δt, while, as preferred by a certain pulsed-lidar manufacturer, $q = 4$ for gates with a Gaussian-shaped weight of the same duration and a threshold equal to e^{-2}.

With this definition we get

Table 1. Summary of dimensionless structure functions and spectra.

	CW anemometer	LIDAR anemometer
$\Delta(\beta, r/\ell)$	$\frac{9}{25}\sqrt{\frac{3}{\pi}}\frac{\Gamma^2(1/3)}{\Gamma(5/6)}\,\sin^{5/3}\beta\,(r/\ell)^{5/3}$ $+\frac{3}{55}\Gamma\left(\frac{1}{3}\right)(7\cos(2\beta)-5)(r/\ell)^2$	$\frac{3\sqrt{3}}{25}\frac{\Gamma(1/6)\pi}{\Gamma^2(2/3)}\,\sin^{5/3}\beta\,(r/\ell)^{5/3}$ $+\frac{9\Gamma(2/3)}{110}(7\cos(2\beta)-5)(r/\ell)^2$
$f(\beta, k\ell)$	$\frac{1}{5\sqrt{\pi}}\frac{\Gamma(1/3)}{\Gamma(5/6)}\sin^{5/3}\beta\,(k\ell)^{-5/3}$ $+\frac{9}{110}(7\cos(2\beta)-5)\exp(-k\ell)(k\ell)^{-2/3}$	$\frac{\sqrt{3}}{30}\frac{\Gamma(1/6)}{\Gamma(2/3)}\sin^{5/3}\beta\,(k\ell)^{-5/3}$ $+\frac{9}{110}(7\cos(2\beta)-5)\exp(-k^2\ell^2)(k\ell)^{-2/3}$

$$\Delta(\beta, r/\ell) = \frac{\overline{\mathcal{D}}(l, r, \beta)}{\alpha(\varepsilon\ell)^{2/3}} =$$

$$\frac{3\sqrt{3}}{25}\frac{\Gamma(1/6)\pi}{\Gamma^2(2/3)}\,\sin^{5/3}\beta\,(r/\ell)^{5/3} + \frac{9\Gamma(2/3)}{110}(7\cos(2\beta)-5)(r/\ell)^2 \qquad (70)$$

and

$$f(\beta, k\ell) = \frac{k\overline{\mathcal{F}}(\ell, k, \beta)}{\alpha(\varepsilon\ell)^{2/3}} =$$

$$\frac{\sqrt{3}}{30}\frac{\Gamma(1/6)}{\Gamma(2/3)}\,\sin^{5/3}\beta\,(k\ell)^{-5/3} + \frac{9}{110}(7\cos(2\beta)-5)\exp(-k^2\ell^2)(k\ell)^{-2/3}. \qquad (71)$$

For convenience the results are presented in Table 1.

We recall that these expressions for the structure functions and the spectra were derived under the assumption that $r/\ell \ll 1$ and $k\ell \gg 1$. These assumptions do not by themselves guarantee that the expressions in Table 1 provide acceptable approximations to the true structure functions and spectra. As the equations show, these small-scale expressions are likely to become negative in certain intervals of β and ρ. We now determine the domains in the β-ρ plane where this actually happens. Looking closer into this problem, we note that both structure functions have the form

$$\Delta(\beta, r/\ell) = A\left(\frac{r}{\ell}\right)^{5/3}\left\{C\sin^{5/3}\beta + (7\cos(2\beta)-5)\left(\frac{r}{\ell}\right)^{1/3}\right\}, \qquad (72)$$

where A and C are positive constants.

Similarly, the spectra have the common form

$$f(\beta, k\ell) = A(k\ell)^{-5/3}\left\{C\sin^{5/3}\beta + (7\cos(2\beta)-5)(k\ell)\exp\left(-(k\ell)^n\right)\right\}, \qquad (73)$$

where $n = 1$ for the CW anemometer and $n = 2$ for the LIDAR anemometer, while (A, C) is another set of positive constants.

A detailed analysis of the non-negativity problem for (72) is given in appendix C. Here we shall just show the results.

We summarize the thresholds for which the structure functions and the spectra are guaranteed positive in Table 2.

Table 2. Thresholds for structure functions and spectra in the inertial subrange.

	CW anemometer	LIDAR anemometer
$(r/\ell)\|_{\max}$	2.075	3.314
$(k\ell)\|_{\min}$	1.985	1.296

The expressions for the spectra in Table 1 allow us to calculate in an easy way the low-pass filtered variance from any lower wave-number limit which does not conflict with the requirement that the spectra are non-negative.

The general formulation (73) will also allow us to determine the intervals of β for which the spectrum is never negative, although this has probably little practical relevance. Again the details are found in appendix C. The result is that we for the the CW-laser anemometer find that the spectrum is never negative for $0° \leq \beta \leq 44.9°$. For the lidar anemometer the corresponding interval is $0° \leq \beta \leq 35.6°$.

The domains for which both the local-isotropy structure function and the spectrum in Table 1 are negative are displayed as contour plots in Figs. 4 and 5.

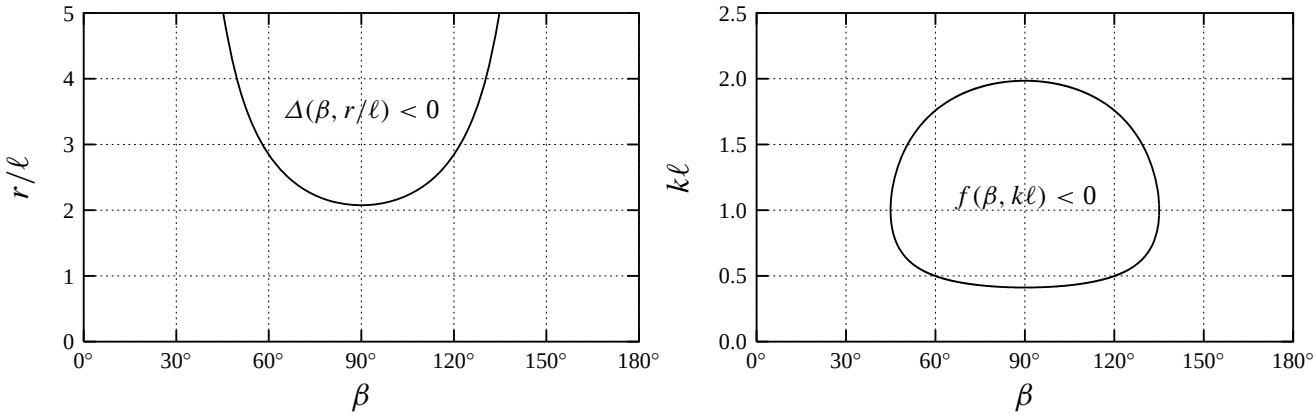

Figure 4. Negative domains of the structure function and the spectrum for the CW laser anemometer. Left frame: Structure function. Right frame: Spectrum.

We believe that the presence of the negative domains obtained from this analysis is not likely to be the only limiting factor for using the model expressions in Table 1.

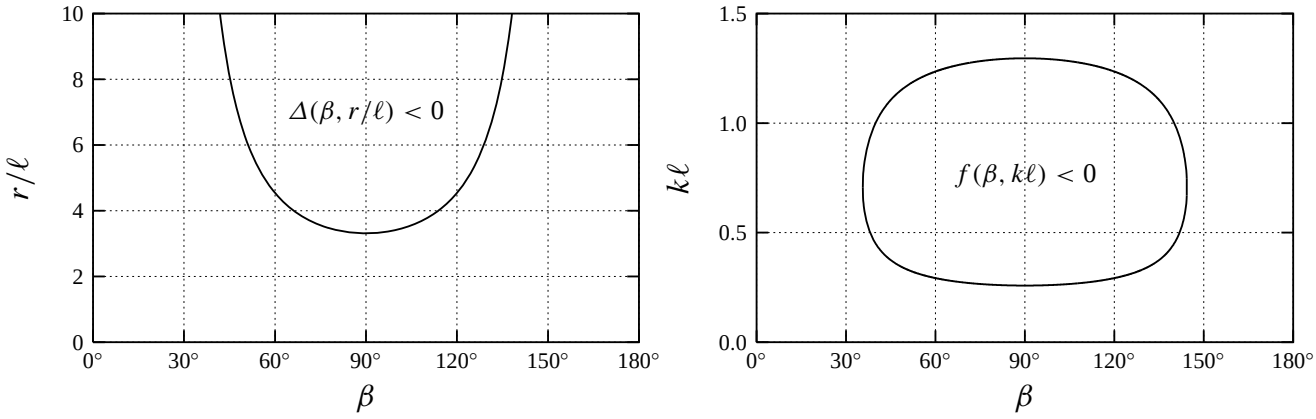

Figure 5. Negative domains of the structure function and the spectrum for the LIDAR anemometer. Left frame: Structure function. Right frame: Spectrum.

5 Conclusion

We have discussed the properties of the signals from two types of laser anemometers, the CW-laser anemometer and the lidar anemometer, which operate on basis of two different modes. They both measure the wind-velocity component along the laser beam by back scattering, but the first measures constantly in time with its focus at one particular distance whereas the second operates by sending pulses of a certain duration and range gating the returned signal. The last can be used to measure simultaneously, at sampling and processing time, the velocity at several distances, albeit with a certain dead time, typically 1 s, between each wind speed determination.

Both anemometers measure the velocity component with a line averaging along the laser beam. The corresponding filters are different, but can in both cases be characterized by one length ℓ of about 20–30 m. In our analysis we have assumed that the velocity turbulence is locally isotropic. The advantage is that the outer length scale, or integral scale, of the turbulence does not enter. In other words, the large eddies are excluded and this means that we cannot predict velocity spectra for low wave numbers below the inertial subrange. Further, in the case of the lidar anemometer the discrete sampling in time implies that the spectra at high wave numbers are biased by aliasing as discussed by Kristensen et al. (2010). However, the measured structure functions and spectra might be useful for the determination of the small-scale turbulence in terms of the dissipation ε.

We have found that there are striking similarities between the two types of anemometers what expressions for both structure functions and spectra are concerned. In section 4 we have compared the structure functions for small displacements $\rho = r/\ell$ and the spectra for corresponding large wave numbers $\kappa = k\ell$. The approximations in the limits $\rho \to 0$ and $\kappa \to \infty$ reveals that in certain domains the structure functions and the spectra become negative. These domains are shown and are useful to specify the limits of validity of the small-eddy approximations which has been assumed. It is also possible to test how different the limiting expression (67) and (70) deviate from the results obtained by numerical integrations of (42) and (58) which, of course cannot result in negative results. Figure 6 shows the ratio of the limiting expressions and the results of numerical integration as functions of ρ with the angle β between the mean-wind direction and the beam direction as a parameter. We see that if we require an offset smaller than 10% the dimensionless displacement ρ should be no larger than 0.6 for the CW-laser anemometer and no larger than about 1 for the approximate expressions to be acceptable.

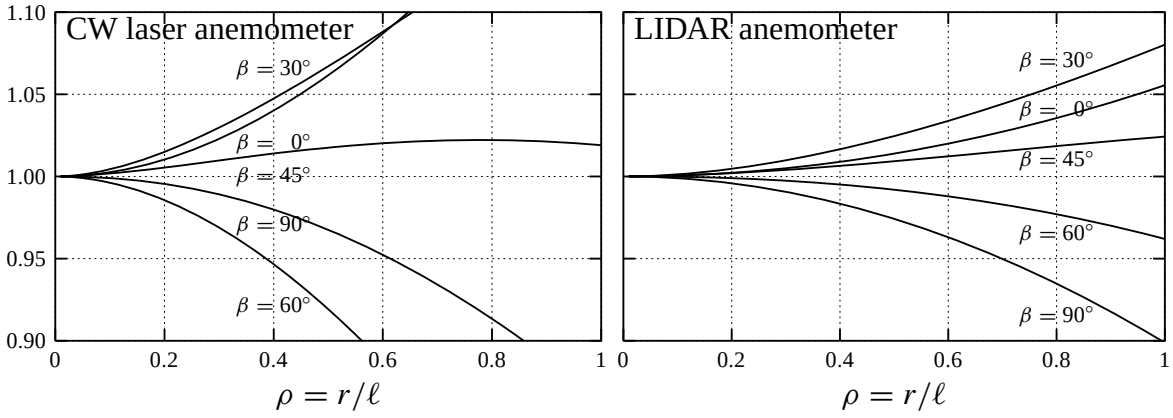

Figure 6. Ratio of structure functions in the limit $\rho \to 0$ to the numerically integrated structure functions for a selection of angles β between the mean-wind direction and the beam direction.

Appendices

A Small Displacements for the CW Anemometer

To obtain an expression for $\overline{\mathcal{D}}(\ell, r, \beta) \equiv \overline{\mathcal{D}}(\rho, \beta)$ in (42) that is useful when $\rho \ll 1$ we shall recast (43) in complex arithmetic form. Applying Euler's formula to the cosine, we obtain

$$\int_0^\infty e^{-a\kappa}(1-\cos(c\kappa))\kappa^{\nu-1}\mathrm{d}\kappa = \Gamma(\nu)\Big(a^{-\nu} - \frac{1}{2}(a-\mathrm{i}\,c)^{-\nu} - \frac{1}{2}(a+\mathrm{i}\,c)^{-\nu}\Big), \quad \text{(A 1)}$$

which is valid when $\nu > -2$ and $\nu \neq 0, -1$, such that the actual case $\nu = -2/3$ is covered. The new form of $\overline{\mathcal{D}}(\rho, \beta)$ becomes

$$\overline{\mathcal{D}}(\rho,\beta) = \frac{3\Gamma(1/6)(\Gamma(1/3))^2 A}{20\pi^{3/2}} \int_0^{2\pi} \Big(1 - \frac{8}{11}\cos^2\Theta\Big)$$

$$\times\Big\{\frac{1}{2}(|\cos\Theta| - \mathrm{i}\,\rho\cos(\Theta+\beta))^{2/3}$$

$$+\frac{1}{2}(|\cos\Theta| + \mathrm{i}\,\rho\cos(\Theta+\beta))^{2/3} - |\cos\Theta|^{2/3}\Big\}\mathrm{d}\Theta, \quad \text{(A 2)}$$

where $A = \alpha(\epsilon l)^{2/3}$. To get rid of the numeric signs in (A 2) we note that $\cos\Theta > 0$ when $\Theta \in (-\pi/2, \pi/2)$, while $\cos\Theta < 0$ when $\Theta \in (\pi/2, 3\pi/2)$. Consequently

$$\overline{\mathcal{D}}(\rho,\beta)=\frac{3\Gamma(1/6)(\Gamma(1/3))^2A}{20\pi^{3/2}}\int\limits_{-\pi/2}^{\pi/2}\Big(1-\frac{8}{11}\cos^2\Theta\Big)\times$$

$$\Big\{(\cos\Theta-\mathrm{i}\,\rho\cos(\Theta+\beta))^{2/3}+(\cos\Theta+\mathrm{i}\,\rho\cos(\Theta+\beta))^{2/3}-2\cos^{2/3}\Theta\Big\}\mathrm{d}\Theta. \quad \text{(A 3)}$$

We need expressions for the integrals

$$I(x)=\int\limits_{-\pi/2}^{\pi/2}(\cos\Theta+\mathrm{i}\,x\sin\Theta)^{2/3}\mathrm{d}\Theta \quad \text{(A 4)}$$

and

$$J(x)=\int\limits_{-\pi/2}^{\pi/2}\cos^2\Theta(\cos\Theta+\mathrm{i}\,x\sin\Theta)^{2/3}\mathrm{d}\Theta \quad \text{(A 5)}$$

It can be shown that

$$I(x)=\frac{6\pi^{3/2}}{\Gamma(1/6)\Gamma(1/3)}(1-x^2)^{1/3}+\frac{3}{5}\sqrt{3}\,(x^2)^{5/6}F\Big(\frac{1}{2},1\,;\frac{11}{6}\,;x^2\Big) \quad \text{(A 6)}$$

and

$$J(x)=\frac{3\pi^{3/2}(5-3x^2)}{4\Gamma(1/6)\Gamma(1/3)(1-x^2)^{2/3}}-\frac{27}{220}\sqrt{3}\,(x^2)^{11/6}F\Big(2,\frac{3}{2}\,;\frac{17}{6}\,;x^2\Big), \quad \text{(A 7)}$$

where F is the usual Gaussian hypergeometric function. These formulas are easily derived for $x\in(0,1)$ and can be extended to $x\in\mathbb{C}$ provided the integration path does not cross a branch point for the integrand. Both I and J are even functions. Returning to (A 3) we find

$$\int\limits_{-\pi/2}^{\pi/2}\Big(1-\frac{8}{11}\cos^2\Theta\Big)\cos^{2/3}\Theta\mathrm{d}\Theta=\frac{36}{11}\frac{\pi^{3/2}}{\Gamma(1/6)\Gamma(1/3)}. \quad \text{(A 8)}$$

We note that

$$\cos\Theta\mp\mathrm{i}\,\rho\cos(\Theta+\beta)=(1\mp\mathrm{i}\,\rho\cos\beta)\Big(\cos\Theta\pm\frac{\mathrm{i}\,\rho\sin\beta\sin\Theta}{1\mp\mathrm{i}\,\rho\cos\beta}\Big) \quad \text{(A 9)}$$

such that, by defining

$$f(\rho)=\frac{1}{2}(1-\mathrm{i}\,\rho\cos\beta)^{2/3}\Big\{I\Big(\frac{\rho\sin\beta}{1-\mathrm{i}\,\rho\cos\beta}\Big)-\frac{8}{11}J\Big(\frac{\rho\sin\beta}{1-\mathrm{i}\,\rho\cos\beta}\Big)\Big\}, \quad \text{(A 10)}$$

(A 3) can be written

$$\overline{\mathcal{D}}(\rho,\beta)=A\Big\{\frac{3\Gamma(1/6)(\Gamma(1/3))^2}{10\pi^{3/2}}(f(\rho)+f(-\rho))-\frac{54}{55}\,\Gamma\Big(\frac{1}{3}\Big)\Big\}. \quad \text{(A 11)}$$

We infer from (A 6)–(A 7) and (A 10)–(A 11) that for small r or ρ,

$$\overline{\mathcal{D}}(\rho,\beta) = d_0 + d_{5/3}\rho^{5/3} + d_2\rho^2 + d_{11/3}\rho^{11/3} + d_4\rho^4 + \cdots . \tag{A 12}$$

No terms of the type d_{1+2p}, ρ^{1+2p} or $d_{2/3+2p}\,\rho^{2/3+2p}$ occur because the corresponding contributions from $1 \pm \mathrm{i}\,\rho\cos\beta$ cancel. We shall evaluate d_0, $d_{5/3}$, and d_2.

To do this we use the following series expansions:

$$(1 - \mathrm{i}\,\rho\cos\beta)^{2/3} = 1 - \frac{2}{3}\,\mathrm{i}\,\cos\beta\cdot\rho + \frac{1}{9}\cos^2\beta\cdot\rho^2 + \cdots \tag{A 13}$$

$$(1 + \mathrm{i}\,\rho\cos\beta)^{2/3} = 1 + \frac{2}{3}\,\mathrm{i}\,\cos\beta\cdot\rho + \frac{1}{9}\cos^2\beta\cdot\rho^2 + \cdots \tag{A 14}$$

$$I(x) = 6\frac{\pi^{3/2}}{\Gamma(1/6)\Gamma(1/3)} + \frac{3}{5}\sqrt{3}x^{5/3} - 2\frac{\pi^{3/2}}{\Gamma(1/6)\Gamma(1/3)}x^2 + \mathcal{O}(x^{11/3}) \tag{A 15}$$

$$J(x) = \frac{15}{4}\frac{\pi^{3/2}}{\Gamma(1/6)\Gamma(1/3)} + \frac{1}{4}\frac{\pi^{3/2}}{\Gamma(1/6)\Gamma(1/3)}x^2 + \mathcal{O}(x^{11/3}) \tag{A 16}$$

Then we find, as expected, that $d_0 = 0$. To find $d_{5/3}$ we note that the only 5/3-term in $I(x)$ or $J(x)$ is located in (A 15). We obtain:

$$d_{5/3} = A\frac{9\sqrt{3}\,\Gamma(1/6)(\Gamma(1/3))^2}{50\pi^{3/2}}\sin^{5/3}\beta \tag{A 17}$$

It remains to evaluate d_2. This can be derived from (A 13)–(A 16) in connection with (A 10) and (A 11). The result is

$$d_2 = A\frac{3}{55}\Gamma(1/3)\,(7\cos 2\beta - 5) \tag{A 18}$$

We have thus established the truth of (50).

B Small Displacements for the LIDAR Anemometer

We want to find an asymptotic expression of the structure function (58) when the dimensionless displacement length $\rho = r/\ell$ is small. This expression should be based on (59). We shall use a free context-dependent parameterization of function arguments. As the subsequent analysis will show, the asymptotic form of $\overline{\mathcal{D}}$ is as follows when $\rho \to 0$:

$$\overline{\mathcal{D}}(\rho,\beta) = \rho^{5/3}(a_0 + a_1\rho^2 + a_2\rho^4 + \cdots) + b_1\rho^2 + b_2\rho^4 + \cdots , \tag{B 1}$$

where the coefficients $a_0, a_1, \ldots, b_1, b_2, \ldots$ are independent of ρ but depend on β. We only want to determine a_0 and b_1. This turned out to be a difficult task. (Maybe there exist easier ways than our method.) Making a series expansion in ρ of (59) will not work, since this results in a $(\cos\Theta)^{-4/3}$ singularity which makes (58) diverge. Since (60) is periodic in Θ with period π, the structure function can be written

$$\overline{\mathcal{D}}(\rho,\beta) = K \int_{-\pi/2}^{\pi/2} \cos^{2/3}\Theta \left(1 - \frac{8}{11}\cos^2\Theta\right)$$

$$\times \left({}_1F_1\Big(-\frac{1}{3};\frac{1}{2};-\frac{1}{4}\cos^2(\Theta+\beta)\sec^2\Theta\,\rho^2\Big) - 1\right) \mathrm{d}\Theta, \quad \text{(B 2)}$$

where

$$K = \alpha(\varepsilon\ell)^{2/3}\frac{2\sqrt{3\pi}}{5\Gamma(5/6)}. \quad \text{(B 3)}$$

We shall first find the dominant term of the asymptotic form of (B 2) when $\rho \to 0$, corresponding to a_0 in (B 1). Clearly the limit value itself is 0. For small ρ the ${}_1F_1 - 1$ term in (B 2) is small except when $\Theta \to \pm\frac{1}{2}\pi$ where ${}_1F_1 \to +\infty$ for fixed ρ. Thus, since the significant contributions come from Θ-values near $\pm\frac{1}{2}\pi$, the leading part of the asymptotic form is unaffected of the factor $1 - \frac{8}{11}\cos^2\Theta$ in (B 2). For the same reason we can make the replacement $\cos^2(\Theta+\beta) \approx \sin^2\beta$. Defining

$$\tau = \frac{1}{4}\sin^2\beta\,\rho^2 \quad \text{(B 4)}$$

we can then replace (B 2) with the approximation

$$\overline{\mathcal{D}}(\tau) = K\Big(f(\tau) - \frac{\sqrt{\pi}\Gamma(5/6)}{\Gamma(4/3)}\Big), \quad \text{(B 5)}$$

where

$$f(\tau) = \int_{-\pi/2}^{\pi/2} \cos^{2/3}\Theta\ {}_1F_1\Big(-\frac{1}{3};\frac{1}{2};-\tau\sec^2\Theta\Big)\,\mathrm{d}\Theta. \quad \text{(B 6)}$$

For the ${}_1F_1$ we shall use the Mellin-Barnes contour integral (Erdélyi et al. 1953, Vol. 1, p, 256):

$${}_1F_1(a;c;-z) = \frac{1}{2\pi\,\mathrm{i}}\frac{\Gamma(c)}{\Gamma(a)}\int_{\gamma-\mathrm{i}\infty}^{\gamma+\mathrm{i}\infty}\frac{\Gamma(-s)\Gamma(a+s)}{\Gamma(c+s)}z^s\mathrm{d}s, \quad \text{(B 7)}$$

which is valid for $|\arg z| < \frac{1}{2}\pi$ and $a, c \neq 0, -1, -2, \ldots$. Moreover the contour must separate the poles of $\Gamma(-s)$ from those of $\Gamma(a+s)$. We insert this in (B 6) and reverse the integration order, and carrying out the Θ-integration we find

$$f(\tau) = \frac{\pi}{\Gamma(-1/3)}\frac{1}{2\pi\,\mathrm{i}}\int_{-\mathrm{i}\infty}^{\mathrm{i}\infty}\frac{\Gamma(-s)\Gamma(5/6-s)\Gamma(-1/3+s)}{\Gamma(1/2+s)\Gamma(4/3-s)}\tau^s\mathrm{d}s \quad \text{(B 8)}$$

This can be written in terms of a Meijer G-function (Erdélyi et al. 1953, Vol. 1, p, 207):

$$f(\tau) = \frac{\pi}{\Gamma(-1/3)}G^{21}_{23}\left(\tau\,\middle|\,\begin{matrix}4/3, & 4/3 \\ 0, & 5/6, \quad 1/2\end{matrix}\right), \quad \text{(B 9)}$$

where we have (Erdélyi et al. 1953, Vol. 1, p, 208)

$$G_{23}^{21}\left(\tau \,\middle|\, \begin{matrix} 4/3, & 4/3 \\ 0, & 5/6, \quad 1/2 \end{matrix}\right) = \frac{\Gamma(5/6)\Gamma(-1/3)}{\Gamma(1/2)\Gamma(4/3)}\,{}_2F_2\Big(-\frac{1}{3}, -\frac{1}{3}; \frac{1}{6}, \frac{1}{2}; -\tau\Big)$$

$$+ \frac{\Gamma(-5/6)}{\Gamma(4/3)}\tau^{5/6}\,{}_2F_2\Big(\frac{1}{2}, \frac{1}{2}; \frac{11}{6}, \frac{4}{3}; -\tau\Big). \qquad \text{(B 10)}$$

For small τ both ${}_2F_2$ approach 1 and hence

$$f(\tau) \approx \frac{\sqrt{\pi}\Gamma(5/6)}{\Gamma(4/3)} + \frac{\pi\Gamma(-5/6)}{\Gamma(-1/3)\Gamma(4/3)}\tau^{5/6} \qquad \text{(B 11)}$$

Inserting this in (B 5) and substituting (B 3) and (B 4) we obtain

$$\overline{D}(\beta, \rho) \approx a_0\rho^{5/3} = C_{5/3}\,\alpha(\varepsilon\ell)^{2/3}(\rho\,\sin\beta)^{5/3}, \qquad \text{(B 12)}$$

where

$$C_{5/3} = \frac{3\sqrt{3}\Gamma(1/6)\pi}{25(\Gamma(2/3))^2} = 1.982196. \qquad \text{(B 13)}$$

Assuming the $(\rho\,\sin\beta)^{5/3}$ factor, it is found by a *Mathematica* fitting-technique, based on numerical integration, that

$$C_{5/3} = 1.98215, \qquad \text{(B 14)}$$

which is in very good agreement with (B 13).

We now switch to finding the next important coefficient b_1 in (B 1). Our procedure for doing this is different from our method of finding a_0. Let us return to (59). Substituting $\kappa = s|\sec\Theta|$ and writing $\xi = \rho\cos(\Theta+\beta)\sec\Theta$ we obtain

$$\Psi(\xi, \Theta) = |\cos\Theta|^{2/3}\int_0^\infty \exp(-s^2)\{1-\cos(\xi s)\}\frac{\mathrm{d}s}{s^{5/3}}. \qquad \text{(B 15)}$$

Since small ρ implies small ξ we shall make a substitution for $1-\cos(\xi s)$ by using the relation

$$\cos x = \mathrm{e}^{-x^2/2} + \mathcal{O}(x^4), \qquad \text{(B 16)}$$

which is valid for small x. This results in an approximately correct expression

$$\Psi_0(\xi, \Theta) = |\cos\Theta|^{2/3}\int_0^\infty \exp(-s^2)\{1-\mathrm{e}^{-\xi^2 s^2/2}\}\frac{\mathrm{d}s}{s^{5/3}}. \qquad \text{(B 17)}$$

Since the dominant parts of both integrals (B 15) and (B 17) come from small s, and since the two integrands agree up to $\mathcal{O}(s^4)$ as $s \to 0$, we expect that using (B 17) will lead to an expansion (B 1) with a correct value of b_1 (and of a_0). The integral (B 17) can be evaluated and gives

$$\Psi_0(\xi, \Theta) = \frac{3}{4}\Gamma(2/3)|\cos\Theta|^{2/3}\Big(-2+2^{2/3}(2+\xi^2)^{1/3}\Big). \qquad \text{(B 18)}$$

By inserting the expression for ξ we obtain

$$\Psi_0(\beta, \rho, \Theta) = \frac{3}{2}\Gamma(2/3)\Big\{\Big(\cos^2\Theta + \frac{1}{2}\cos^2(\beta+\Theta)\,\rho^2\Big)^{1/3} - (\cos^2\Theta)^{1/3}\Big\}, \quad \text{(B 19)}$$

which is integrable over Θ and approximates Ψ for small ρ, though not uniformly over Θ. We substitute Ψ_0 for Ψ in (58), and because the integrand is periodic with period π we get

$$\overline{\mathcal{D}}_0(\beta, \delta) =$$

$$K\int_{-\pi/2}^{\pi/2}\Big(1 - \frac{8}{11}\cos^2\Theta\Big)\Big\{\Big(\cos^2\Theta + \cos^2(\beta+\Theta)\,\delta^2\Big)^{1/3} - \cos^{2/3}\Theta\Big\}\mathrm{d}\Theta, \quad \text{(B 20)}$$

where

$$\delta^2 = \frac{\rho^2}{2} \quad \text{(B 21)}$$

is small. It is a hard problem to find an expression of the main component

$$J = \int_{-\pi/2}^{\pi/2}\Big(1 - \frac{8}{11}\cos^2\Theta\Big)\Big(\cos^2\Theta + \cos^2(\beta+\Theta)\,\delta^2\Big)^{1/3}\mathrm{d}\Theta \quad \text{(B 22)}$$

of the integral in (B 20) that admits an expansion in powers of ρ (or δ). We resolved it by complex integration using an indefinite integral and a half-circular contour. We notice that the integrand is free of singularities in the open integration interval $(-\pi/2, \pi/2)$. By substituting $z = e^{\,\mathrm{i}\,\Theta}$ (B 22) becomes

$$J = \frac{2^{1/3}}{22\,\mathrm{i}}\int(-2 + 7z^2 - 2z^4)\{(1+z^2)^2 + \delta^2(\mathrm{e}^{-\mathrm{i}\,\beta} + \mathrm{e}^{\mathrm{i}\,\beta}z^2)^2\}^{1/3}z^{-11/3}\mathrm{d}z, \quad \text{(B 23)}$$

where the path of integration goes from $-\,\mathrm{i}$ to i. We shall here think of (B 23) as an indefinite integral $F(z)$ taken over limits such that $J = [F(z)]_{-\,\mathrm{i}}^{\,\mathrm{i}}$. The integration can indeed be carried out, although it leads to some less well-known functions. These are Appell's hypergeometric functions in two variables x and y. Appell (1880) introduced 4 such functions, F_1, F_2, F_3, F_4, where only F_1 is required here. Appell's F_1 is defined in terms of its double hypergeometric series:

$$F_1(a, b_1, b_2, c; x, y) = \sum_{m,n}\frac{(a)_{m+n}(b_1)_m(b_2)_n}{m\,!\,n\,!\,(c)_{m+n}}x^m y^n \quad \text{(B 24)}$$

(Erdélyi et al. 1953, Vol. 1, p, 222). In (B 24) the summations extend from m and $n = 0$ to ∞, and $(a)_m$ stands for the Pochhammer symbol $(a)_m = \Gamma(a+m)/\,\Gamma(a)$. To evaluate (B 23) we start with the prototype integral

$$I(x, y, \mu, \nu) = \int f(z)\mathrm{d}z, \quad \text{(B 25)}$$

where

$$f(z) = (1 + xz^2)^{\nu-1}(1 + yz^2)^{\nu-1}z^{\mu-1}. \quad \text{(B 26)}$$

We want to evaluate (B 25) over a semicircle with z going counterclockwise from $-\mathrm{i}$ to $+\mathrm{i}$, while x, y, μ, ν are fixed parameters. By expanding (B 26) in powers of z we obtain

$$f(z) = \sum_{m=0}^{\infty}\sum_{n=0}^{\infty}\binom{\nu-1}{m}\binom{\nu-1}{n}x^m y^n z^{2m+2n+\mu-1}. \tag{B 27}$$

Since

$$\int z^{2m+2n+\mu-1}\mathrm{d}z = \frac{(-1)^{m+n}}{2m+2n+\mu}[z^\mu]_{-\mathrm{i}}^{+\mathrm{i}} \tag{B 28}$$

and $z^\mu = e^{\mu \log z}$, $\log z = \ln|z| + \mathrm{i}\arg z = \mathrm{i}\arg z$, we find

$$[z^\mu]_{-\mathrm{i}}^{+\mathrm{i}} = e^{\mu\,\mathrm{i}\frac{\pi}{2}} - e^{-\mu\,\mathrm{i}\frac{\pi}{2}} = 2\,\mathrm{i}\sin\Big(\mu\frac{\pi}{2}\Big). \tag{B 29}$$

Thus the result becomes

$$I(x,y,\mu,\nu) = \mathrm{i}\sin\Big(\mu\frac{\pi}{2}\Big)\sum_{m=0}^{\infty}\sum_{n=0}^{\infty}\binom{\nu-1}{m}\binom{\nu-1}{n}\frac{(-1)^{m+n}}{m+n+\frac{1}{2}\mu}x^m y^n. \tag{B 30}$$

This can be expressed in terms of an Appell F_1 function (B 24):

$$I(x,y,\mu,\nu) = \frac{2\,\mathrm{i}}{\mu}\sin\Big(\mu\frac{\pi}{2}\Big)F_1\Big(\frac{1}{2}\mu, 1-\nu, 1-\nu, \frac{1}{2}\mu+1; x, y\Big). \tag{B 31}$$

Let us write (B 23) as follows,

$$J = \frac{2^{1/3}}{22\,\mathrm{i}}\int(-2+7z^2-2z^4)(A+Bz^2+Cz^4)^{1/3}z^{-11/3}\mathrm{d}z, \tag{B 32}$$

where

$$(A,B,C) = (1+\delta^2 e^{-2\,\mathrm{i}\beta}, 2(1+\delta^2), 1+\delta^2 e^{2\,\mathrm{i}\beta}). \tag{B 33}$$

Moreover define

$$D = \sqrt{B^2-4AC}. \tag{B 34}$$

Now we have the identity

$$A+Bz^2+Cz^4 = A(1+xz^2)(1+yz^2) \tag{B 35}$$

with

$$(x,y) = \Big(\frac{2C}{B+D}, \frac{2C}{B-D}\Big). \tag{B 36}$$

By inserting (B 33) in (B 34) we obtain $D = 4\sin\beta\,\delta$ and then

$$(x,y) = \Big(\frac{1+\delta^2 e^{2\,\mathrm{i}\beta}}{1+2\delta\sin\beta+\delta^2}, \frac{1+\delta^2 e^{2\,\mathrm{i}\beta}}{1-2\delta\sin\beta+\delta^2}\Big). \tag{B 37}$$

Using (B 35) we can write (B 32) as

$$J = \frac{2^{1/3}}{22\,\mathrm{i}} A^{1/3} \int (1+xz^2)^{1/3}(1+yz^2)^{1/3}(-2z^{-\frac{11}{3}} + 7z^{-5/3} - 2z^{1/3})\mathrm{d}z \quad \text{(B 38)}$$

and then we see from (B 25)–(B 26) that (B 30) can be used with $\nu = 4/3$ and $\mu = -8/3, -2/3, 4/3$, respectively. In this way we find after reduction:

$$J = \frac{3\sqrt{3}}{88} 2^{1/3} A^{1/3} \Big\{ F_1\Big(-\frac{4}{3}, -\frac{1}{3}, -\frac{1}{3}, -\frac{1}{3}; x, y\Big)$$

$$+ 14F_1\Big(-\frac{1}{3}, -\frac{1}{3}, -\frac{1}{3}, \frac{2}{3}; x, y\Big) - 2F_1\Big(\frac{2}{3}, -\frac{1}{3}, -\frac{1}{3}, \frac{5}{3}; x, y\Big)\Big\}. \quad \text{(B 39)}$$

Since δ is small we have

$$(x, y) \approx (1, 1). \quad \text{(B 40)}$$

Unfortunately (1, 1) belongs to the hardest singularities of F_1 in the entire xy-plane. This means that (B 39) is useless as it stands for obtaining asymptotic results for J when $\rho \to 0$. What we need is a formula for analytic continuation of F_1 into the convergence regions. Such formulas exist but are more complicated than their counterparts for the usual one-dimensional hypergeometric function. We shall use a formula by Olsson (1964)

$$F_1(a, b_1, b_2, c; x, y) =$$

$$\frac{\Gamma(c)\Gamma(c-a-b_1-b_2)}{\Gamma(c-a)\Gamma(c-b_1-b_2)} F_1(a, b_1, b_2, 1+a+b_1+b_2-c; 1-x, 1-y)$$

$$+ \frac{\Gamma(c)\Gamma(a+b_2-c)}{\Gamma(a)\Gamma(b_2)} (1-x)^{-b_1}(1-y)^{c-a-b_2}$$

$$\times F_1\Big(c-a, b_1, c-b_1-b_2, c-a-b_2+1; \frac{1-y}{1-x}, 1-y\Big)$$

$$+ \frac{\Gamma(c)\Gamma(c-a-b_2)\Gamma(a+b_1+b_2-c)}{\Gamma(a)\Gamma(b_1)\Gamma(c-a)} (1-x)^{c-a-b_1-b_2}$$

$$\times G_2\Big(c-b_1-b_2, b_2, a+b_1+b_2-c, c-a-b_2; x-1, \frac{1-y}{x-1}\Big), \quad \text{(B 41)}$$

where

$$G_2(a_1, a_2, b_1, b_2; x, y) = \sum_{m,n} \frac{(a_1)_m (a_2)_n (b_1)_{n-m} (b_2)_{m-n}}{m!\,n!} x^m y^n, \quad \text{(B 42)}$$

and where the m and n summations go from 0 to ∞ (Erdélyi et al. 1953, Vol. 1, p, 224). In (B 41) we put $b_1 = b_2 = -1/3$ and $c = a + 1$. Then (B 41) becomes

$$F_1\Big(a, -\frac{1}{3}, -\frac{1}{3}, a+1; x, y\Big) = \frac{\Gamma(a+1)\Gamma(5/3)}{\Gamma(a+5/3)} F_1\Big(a, -\frac{1}{3}, -\frac{1}{3}, -\frac{2}{3}; 1-x, 1-y\Big)$$

$$- \frac{3}{4} a (1-x)^{1/3}(1-y)^{4/3} F_1\Big(1, -\frac{1}{3}, a+\frac{5}{3}, \frac{7}{3}; \frac{1-y}{1-x}, 1-y\Big)$$

$$+ a \frac{\Gamma(4/3)\Gamma(-5/3)}{\Gamma(-1/3)} (1-x)^{5/3} G_2\Big(a+\frac{5}{3}, -\frac{1}{3}, -\frac{5}{3}, \frac{4}{3}; x-1, \frac{1-y}{x-1}\Big). \quad \text{(B 43)}$$

The function arguments are $\mathcal{O}(\delta)$ in the first F_1. Thus the first addent in (B 43) is analytic and corresponds to the regular part of (B 1), while the two other addents are non-analytic and correspond to the irregular part of (B 1); this indeed confirms the stated structure of the expression (B 1). Here we shall only need the regular part of LHS(B 43):

$$F_1^{\mathrm{reg}}\Big(a, -\frac{1}{3}, -\frac{1}{3}, a+1; x, y\Big)$$

$$= \frac{\Gamma(a+1)\Gamma(5/3)}{\Gamma(a+5/3)} F_1\Big(a, -\frac{1}{3}, -\frac{1}{3}, -\frac{2}{3}; 1-x, 1-y\Big). \tag{B 44}$$

We are now in a position to compute the leading δ^2-term of the regular part of J in (B 39). To do this we insert (B 37) into (B 44). A series expansion in δ yielded the following result:

$$J_{\mathrm{reg}} = \frac{6\sqrt{\pi}\Gamma(5/6)}{11\Gamma(4/3)}\Big(1 + \frac{1}{6}(7\cos 2\beta - 5)\delta^2 + \cdots\Big). \tag{B 45}$$

Going back to (B 20) we notice that

$$-\int_{-\pi/2}^{\pi/2} \Big(1 - \frac{8}{11}\cos^2\Theta\Big)\cos^{2/3}\Theta \,\mathrm{d}\Theta = -\frac{6\sqrt{\pi}\Gamma(5/6)}{11\Gamma(4/3)} \tag{B 46}$$

annihilates the constant term in (B 45) such that by using (B 3) and (B 21) this can be written

$$\overline{\mathcal{D}}_{\mathrm{reg}}(\rho, \beta) \approx b_1\rho^2 = C_2\alpha(\varepsilon\ell)^{2/3}(7\cos 2\beta - 5)\rho^2, \tag{B 47}$$

where

$$C_2 = \frac{9}{110}\Gamma\Big(\frac{2}{3}\Big) = 0.1107915 \tag{B 48}$$

Assuming the $(7\cos 2\beta - 5)\rho^2$ behavior, it was possible to reproduce (B 48). A *Mathematica* fitting technique based on numerical integration resulted in

$$C_2 = 0.110582. \tag{B 49}$$

C Negative Domains of the Structure Functions and Spectra

We investigate the conditions under which the structure function Δ in (72) and the spectrum f in (73) stay non-negative. Beginning with the structure function we need only consider the following factor,

$$D(\beta, \rho) = C\sin^{5/3}\beta + (7\cos 2\beta - 5)\rho^{1/3}, \tag{C 1}$$

where $\rho = r/\ell$ and $\beta \in [0, \pi]$. Here C depends on the anemometer type:

$$\text{CW:} \qquad C = \frac{33\Gamma(1/3)}{5\Gamma(5/6)}\sqrt{\frac{3}{\pi}} = 15.306658 \tag{C 2}$$

and

$$\text{LIDAR:} \qquad C = \frac{22\pi\,\Gamma(1/6)}{5\sqrt{3}\Gamma^3(2/3)} = 17.891234. \tag{C 3}$$

The boundary curve enclosing the negativity range for the structure function is the zero contour for the function $D(\beta, \rho)$ and is shown in the left frames of Figs. 4 and 5 for CW and LIDAR, respectively. We are particularly interested in the maximum value of $\rho = r/\ell$ for which $D(\beta, \rho) \geq 0$ for all $\beta \in [0, \pi]$. Since $D(\pi - \beta, \rho) = D(\beta, \rho)$ it is sufficient to study the sign of D when β varies in the interval $[0, \pi/2]$. Let us substitute

$$\sin\beta = \sigma, \quad \sigma \in [0, 1]. \tag{C 4}$$

Writing $d(\sigma) = D(\beta, \rho)$, (C 1) becomes

$$d(\sigma) = C\sigma^{5/3} + (2 - 14\sigma^2)\rho^{1/3}. \tag{C 5}$$

In particular

$$d(1) = C - 12\rho^{1/3}. \tag{C 6}$$

The derivative of (C 5) is

$$d'(\sigma) = \frac{1}{3}\Big(5C - 84\rho^{1/3}\sigma^{1/3}\Big)\sigma^{2/3}, \tag{C 7}$$

which is zero when $\sigma = \sigma_0 = 125C^3/(592704\rho)$. If $\sigma_0 \geq 1$ then (C 7) is everywhere positive when $\sigma \in (0, 1)$, and d is strictly increasing in the same interval. On the other hand, if d goes negative somewhere when $\sigma \leq 1$, its minimum is attained at $\sigma = 1$ ($\beta = \pi/2$) and equals (C 6). Consequently $D(\beta, \rho)$ (or Δ) is non-negative for all β if and only if $d(1) \geq 0$, or

$$\rho \leq \Big(\frac{C}{12}\Big)^3. \tag{C 8}$$

This means that the largest "legal" value of $\rho = r/\ell$ for any angle β is obtained by solving $d(1) = 0$ or $D(\pi/2, r/\ell) = 0$, i.e.

$$C\sin^{5/3}(\pi/2) + (7\cos(2\pi/2) - 5)\Big(\frac{r}{\ell}\Big)^{1/3} = 0. \tag{C 9}$$

The result is of course

$$\rho_{\max} = \frac{r}{\ell}\Big|_{\max} = \Big(\frac{C}{12}\Big)^3. \tag{C 10}$$

By inserting (C 2) and (C 3) in (C 10) we reproduce the line labeled $(r/\ell)|_{\max}$ in Table 2.

A similar analysis can be made for the spectrum f. Here we consider the factor

$$F(\beta, \kappa) = C\sin^{5/3}\beta + (7\cos 2\beta - 5)\kappa\exp(-\kappa^n), \tag{C 11}$$

where $\kappa = k\ell$. Moreover $n = 1$ for CW and $n = 2$ for LIDAR. C too depends on the anemometer type:

$$\text{CW:} \qquad C = \frac{22\Gamma(1/3)}{9\sqrt{\pi}\Gamma(5/6)} = 3.2730751 \tag{C 12}$$

and

$$\text{LIDAR:} \qquad C = \frac{11\Gamma(1/6)}{9\sqrt{3}\Gamma(2/3)} = 2.9006873. \tag{C 13}$$

The boundary curve enclosing the negativity range for the spectrum is the zero contour for the function $F(\beta, \kappa)$ and is shown in the right frames of Figs. 4 and 5 for CW and LIDAR, respectively. As the same figures indicate, $F(\beta, \kappa)$ is non-negative for all $\beta \in [0, \pi]$ when $\kappa = k\ell$ is large. We are interested in finding the minimum value $\kappa = \kappa_2$ with this property. (Furthermore, $F(\beta, \kappa)$ is non-negative for all $\beta \in [0, \pi]$ when κ is small, and there exist a maximum value $\kappa = \kappa_1$ with this property but this is not very interesting from a practical point of view.) We substitute (C 4) and obtain by defining $\phi(\sigma) = F(\beta, \kappa)$

$$\phi(\sigma) = C\sigma^{5/3} + (2 - 14\sigma^2)\kappa \exp(-\kappa^n). \tag{C 14}$$

In particular

$$\phi(1) = C - 12\kappa \exp(-\kappa^n). \tag{C 15}$$

The derivative of (C 14) is

$$\phi'(\sigma) = \frac{1}{3}\Big(5C - 84\kappa \exp(-\kappa^n)\sigma^{1/3}\Big)\sigma^{2/3}, \tag{C 16}$$

which is zero when $\sigma = \sigma_0 = 125C^3/(592704(\kappa \exp(-\kappa^n))^3)$. If $\sigma_0 \geq 1$ then (C 16) is everywhere positive when $\sigma \in (0, 1)$, and ϕ is strictly increasing in the same interval. If ϕ goes negative when $\sigma \leq 1$, its minimum value is attained at $\sigma = 1$ ($\beta = \pi/2$) and equals (C 15). Consequently $F(\beta, \kappa)$ (or f) is non-negative for all β if and only if

$$\kappa \exp(-\kappa^n) \leq \frac{C}{12}. \tag{C 17}$$

Let M be the maximum of LHS(C 17), attained at $\kappa = \kappa^*$. We find

$$(M, \kappa^*) = \Big(\frac{1}{\sqrt[n]{ne}}, \frac{1}{\sqrt[n]{n}}\Big) \qquad n = 1, 2. \tag{C 18}$$

This gives for the two anemometer types:

$$\text{CW:} \qquad (M, \kappa^*) = \Big(\frac{1}{e}, 1\Big) \tag{C 19}$$

$$\text{LIDAR:} \qquad (M, \kappa^*) = \Big(\frac{1}{\sqrt{2e}}, \frac{1}{\sqrt{2}}\Big). \tag{C 20}$$

The numerical values of M and $C/12$ are:

	CW	LIDAR
M	0.367879	0.428882
$C/12$	0.272756	0.241724

(C 21)

and so by (C 17) it is indeed confirmed that there exist (β, κ)-values for which $F(\beta, \kappa) < 0$. The abovementioned numbers κ_1 and κ_2 are the roots of the equation

$$\kappa \exp(-\kappa^n) = \frac{C}{12}. \tag{C 22}$$

We find

	CW	LIDAR
κ_1	0.411689	0.258417
κ_2	1.98459	1.29579

. (C 23)

The values of κ_2 are the more important of the two sets, and they are retrieved in the lower line of Table 2 as $kl|_{\min}$. We shall finally determine $\beta = \beta_{\max} \in (0, \pi/2)$ as the maximum angle for which the spectrum is never negative. The line $\beta = \beta_{\max}$ is a vertical tangent to the closed contour in Figs. 4 or 5. The corresponding ordinate $\kappa = k\ell$ is equal to κ^* in (C 18) and is a double root of (C 22) whose LHS for this value attains its maximum M as given by (C 18). Hence to find $\beta_{\max}$ (or σ) we just replace $\kappa \exp(-\kappa^n)$ in (C 14) with M:

$$C\sigma^{5/3} + (2 - 14\sigma^2)\frac{1}{\sqrt[n]{n\,e}} = 0. \tag{C 24}$$

Setting $s = \sigma^{1/3}$ we obtain an algebraic equation of degree 6:

$$14s^6 - \sqrt[n]{n\,e}\,C\,s^5 - 2 = 0. \tag{C 25}$$

This can be solved numerically for CW or LIDAR. In both cases there is just one positive root, and we find:

	CW	LIDAR
s	0.890551	0.835012
σ	0.706278	0.582209
$\beta_{\max}$	44.9329°	35.6061°

. (C 26)

These $\beta_{\max}$ values were also reported in section 4.

Acknowledgements

The authors are grateful for the support to the WindScanner project from the Danish Strategic Research Council, Danish Agency for Science -Technology and Innovation; Research Infrastructure 2009; Grant No. 2136-08-0022.

References

Banakh, V. A. & Smalikho, I. N. (1997), 'Determination of the turbulent energy dissipation rate from lidar sensing data', *Atmos. Oceanic Opt.* **10**, 295–302.

Banakh, V. A., Smalikho, I. N., Köpp, F. & Werner, C. (1999), 'Measurements of turbulent energy dissipation rate with a cw doppler lidar in the atmospheric boundary layer', *J. Atmos. Ocean. Technol.* **16**, 1044–1061.

Erdélyi, A., Magnus, W., Oberhettinger, F. & Tricomi, F. G. (1953), *Bateman Manuscript Project - Higher Transcendental Functions*, McGraw-Hill Book Company, New York. Vol. 1–3.

Kolmogorov, A. N. (1941), 'The local structure of turbulence in an incompressible viscous fluid for very large Reynolds numbers', *Dokl. Akad. Nauk SSSR* **30**, 9–13.

Kristensen, L., Kirkegaard, P., Fairall, C. W., Kaimal, J. C. & Lenschow, D. H. (1992), Advantages of tapering of finite data records for spectral analysis, Technical Report NOAA Technical Memorandum ERL WPL-226, National Oceanic and Atmospheric Administration, Environmental Research Laboratories.

Kristensen, L., Kirkegaard, P., Mann, J., Mikkelsen, T., Nielsen, M. & Sjöholm, M. (2010), Spectral coherence along a lidar-anemometer beam, Technical Report R-1744(EN), Risø DTU National Laboratory for Sustainable Energy.

Olsson, P. O. M. (1964), 'Integration of partial differential equations for the hypergeometric functions f_1 and f_d of two and more variables', *J. Math. Phys.* **5**, 420–430.

Smalikho, I. N. (1995), 'On measurement of the dissipation rate of the turbulent energy with a CW lidar', *Atmos. Oceanic Opt.* **8**, 788–793.

Risø DTU is the National Laboratory for Sustainable Energy. Our research focuses on development of energy technologies and systems with minimal effect on climate, and contributes to innovation, education and policy. Risø has large experimental facilities and interdisciplinary research environments, and includes the national centre for nuclear technologies.

Risø DTU
National Laboratory for Sustainable Energy
Technical University of Denmark

Frederiksborgvej 399
PO Box 49
DK-4000 Roskilde
Denmark
Phone +45 4677 4677
Fax +45 4677 5688

www.risoe.dtu.dk